

7. CALCULATIONS VERSUS MEASUREMENTS

Methods used to analyze experimental data are discussed in Section 6. Here the results from such analyses are compared with corresponding analytical calculations. In many cases, perhaps most, the comparisons are expressed in terms of calculated-to-experiment (C/E) ratios.

7.1 Water and Beryllium-Reflected Criticals with Unirradiated Fuel

Standard approach-to-critical measurements were made in the ORR using cores consisting of unirradiated HEU and LEU fuel reflected with both water and beryllium. Preliminary results from these measurements have been reported.²⁷ More recently, the calculations were repeated using revised EPRI-CELL libraries⁴⁰ and including the effects of minor elements and impurities in the DIF3D calculations. The revised EPRI-CELL library ensured the use of constant weighting for the 35 groups in the thermal energy range. Some materials, such as H(H₂O), had 1/E weighting in the thermal energy range in the old cross section library, which resulted in too much absorption. The absorbing effects of minor elements and impurities in the aluminum structural materials have been expressed in terms of the equivalent parts per million ($\mu\text{g/g}$) of natural boron. For the LEU-1 and LEU-2 cores the standard fuel elements were fabricated by CERCA. The fuel followers and HEU fuel elements used 6061 aluminum alloy for structural material. Table 27 shows the composition of each of the aluminum alloys and the equivalent ppm of natural boron. In addition, the beryllium reflector elements have an equivalent 7.82 ppm of natural boron as determined from a complete chemical analysis of beryllium provided by Brush Wellman, Inc. Results from the revised calculations, including VIM-Monte Carlo comparisons, also have been reported.⁴¹

Fresh critical assemblies were constructed for the purpose of obtaining data to test analytical models and codes. Figure 19 shows the core configuration for the water-reflected criticals with fresh HEU and LEU fuel. Because of excess reactivity considerations, the HEU critical (HEU-1) had no fuel elements in grid positions C4 and C6. For the last LEU critical (179AX5) the MFE experiments were removed from the core and replaced with water.

The HEU and LEU beryllium-reflected cores were of identical geometry and consisted of a 3 x 3 assembly of fuel with shim rods located at each corner position. (See Fig. 20). As before, however, the MFE's were removed for the last beryllium-reflected LEU core (179AX6). For all of the critical configurations shim rods normally located in positions B4 and B6 were removed and replaced with reflector material.

Diffusion and Monte Carlo calculations were performed for each of the unirradiated fuel assemblies with the four banked shim rods located at the experimentally-determined critical rod positions (CRP). For rods withdrawn 15.25" the bottom of the cadmium poison section of the ganged shim rods lies on the core midplane.

Table 28 shows the calculated eigenvalues for the water-reflected criticals. Since the cross section libraries were generated for temperatures different from the experimental conditions, temperature corrections, based on calculated isoLhen-nal temperature coefficients, were applied. The reactivity effect of impurities and minor elements present in aluminum structural materials was represented by equivalent ¹⁰B concentrations in the diffusion calculations. However, a correction for this effect had to be applied to the first set of Monte Carlo calculations which omitted the impurities and minor elements.

Similar results for the beryllium- reflected cores are given in Table 29. For these cases the ⁶Li and ³He poison concentrations were estimated from records available for the irradiation history of each beryllium reflector element. (See Section 5.7).

Table 27. Equivalent ppm Natural Boron for Aluminum Alloys

<u>Element</u>	<u>CERCA-Al₁</u>		<u>6061-Al</u>	
	<u>Wt%</u>	<u>Eq. ppm Boron</u>	<u>Wt%</u>	<u>Eq. ppm Boron</u>
Cu	0.005	0.43	0.275	2.343
Mg	4.92	1.816	1.00	0.369
Mn	0.01	0.345	0.10	3.448
Cr	0.01	0.085	0.195	1.656
Si	0.11	0.089	0.60	0.487
Fe	0.27	1.742	0.60	3.872
Ti	0.01	0.181	0.10	1.814
Zn	0.01	0.024	0.20	0.479
Ni	0.01	0.112	-	-
B	0.001	10.000	0.001	10.000
Li	0.001	1.457	0.001	1.457
Cd	0.001	3.105	0.001	3.105
Al	94.642	117.415	96.927	120.246
Total	100.0	136.414	100.0	149.280
Al (pure)	100.0	124.058	100.0	124.058
	Net ppm:	12.356		25.218

ORR FRESH FUEL CRITICALS

A	H ₂ O								
B	H ₂ O								
C	H ₂ O	H ₂ O	MFE	FE	FE	FE	MFE	H ₂ O	H ₂ O
D	H ₂ O	H ₂ O	FE	SR	FE	SR	FE	H ₂ O	H ₂ O
E	H ₂ O	H ₂ O	FE	FE	FE	FE	FE	H ₂ O	H ₂ O
F	H ₂ O	H ₂ O	FE	SR	FE	SR	FE	H ₂ O	H ₂ O
G	H ₂ O								
	1	2	3	4	5	6	7	8	9

Water-reflected cores HEU-1
 [no fuel elements (FE) in C-4 and C-6],
 LEU-1, and 179-AX5 (without MFE's).

Fig. 19

ORR FRESH FUEL CRITICALS

A	H ₂ O								
B	H ₂ O								
C	H ₂ O	Be	MFE	Be	Be	Be	MFE	Be	H ₂ O
D	H ₂ O	Be	Be	SR	FE	SR	Be	Be	H ₂ O
E	H ₂ O	Be	Be	FE	FE	FE	Be	Be	H ₂ O
F	H ₂ O	Be	Be	SR	FE	SR	Be	Be	H ₂ O
G	H ₂ O	Be	H ₂ O						
	1	2	3	4	5	6	7	8	9

Beryllium-reflected cores HEU-2, LEU-2, and
179-AX6 (without MFE's)

Fig. 20

Table 28. Eigenvalue Calculations for ORR Fresh Fuel Cores

<u>Water-Reflected Cores</u>						
<u>Core</u>	<u>MFE's?</u>	<u>CRP in.</u>	<u>Code</u>	<u>Corrections, % $\delta k/k$</u>		<u>k_{eff}</u>
				<u>Temp.</u>	<u>Boron Eq.</u>	
HEU-1	Yes	17.21	DIF3D:	-0.1861	-	0.9981
			VIM:	-0.1241	-0.9741	1.0027±0.0022
LEU-1	Yes	15.46	DIF3D:	-0.2117	-	0.9959
			VIM:	-0.1411	-0.4199	0.9966±0.0019
179AX5	No	15.48	DIF3D	-0.2156	-	1.0002
			VIM:	-0.1527		1.0027A.0019

Table 29. Eigenvalue Calculations for ORR Fresh Fuel Cores

<u>Beryllium-Reflected Cores</u>						
<u>Core</u>	<u>MFE's?</u>	<u>CRP in.</u>	<u>Code</u>	<u>Corrections, % $\delta k/k$</u>		<u>k_{eff}</u>
				<u>Temp.</u>	<u>Boron Eq</u>	
HEU-2	Yes	17.34	DIF3D:	-0.2070	-	1.0007
			VIM:	-0.1380	-1.2219	1.0032±0.0020
LEU-2	Yes	18.41	DIF3D:	-0.2203	-	0.9959
			VIM:	-0.1469	-0.7785	1.0018±0.0020
179AX6	No	18.22	DIF3D	-0.1769	-	0.9999
			VIM:	-0.1114		1.0022±0.0019

Tables 28 and 29 show that the DIF313-diffusion and the VIM-Monte Carlo eigenvalues agree with each other and with the experimentally-determined critical configurations, for which k_{eff} must equal unity. For purposes of comparison, Fig. 21 shows the DIF3D/VIM reaction rate ratios for the water-reflected critical 179AX5. Similarly, Fig. 22 shows reaction rate ratios for the beryllium-reflected core 179AX6. The DIF313 and VIM reaction rates are consistent for the water-reflected case and for the core region of the beryllium-reflected critical. However, Fig. 22 shows rather large discrepancies in some of the reflector regions of core 179AX6. For this small 3 x 3 core it appears that the model used underestimates the effects of neutron leakage through the voided beam tubes in the radial reflector regions. If the beam tube openings at the outer face of the core box are represented by a set of thin absorbers black to all energy groups, significant improvements result in the reaction rate ratios at locations E1, E2, E8, E9, F2, F8, and G3 to G7. These improvements range from about 4-6%. At the other locations the changes are of the order of 1% or less. The large discrepancy at A5 is thought to be the result of the limitations of diffusion theory to handle deep penetration problems. Because of the small size of the core, the results are quite sensitive to the reflector cross sections, especially for beryllium scattering and (n,2n) reactions. Computational details for cores 179AX5 and 179AX6 are given in Appendix D.

7.2 Cobalt and Gold Activity Distributions

Techniques used for wire activations and methods used to analyze the data are discussed in Sections 4.2.1 and 6.1, respectively. Comparisons of measured activity distributions with calculated ones are given in this section.

Figures 23 and 24 show the fuel-element-averaged C/E ratios for the gold wires activated at very low power in the water-reflected fresh cores HEU-1 and LEU-1. For these two cores the analyses were carried out assuming the beam tubes were flooded with full density water. TWs model underestimates the effect of neutron leakage through the beam tubes on the neutron flux distribution, particularly in the G-row and to a lesser extent in the F-row. The RMS-DEV of the C/E ratios from unity was 6.3% for the HEU core and 5.1% for the LEU core. The gold wire data at position F3 in core HEU-1 was defective and could not be used in the analysis. Appendix G illustrates the evaluation of the gold wire data for core LEU-1.

Figures 25 and 26 show the C/E ratios for the all-HEU core 174C used at the beginning of the demonstration and the experimental core 174FX. The effect on the C/E ratios for wire cross sections generated for the core region and for the beryllium reflector region is seen in Fig. 25. For reasons discussed in Section 6.1, the RMS DEV of the C/E ratios from unity include only those wires activated in standard fuel elements. Except for the europium activation facilities in the beryllium reflector, the low power experimental core 174FX was identical to core 174F which was later operated at 30 MW. For core 174C the voided beam tubes were modeled with a water composition corresponding to 3% of normal density. However, core 174FX used the old model in which the beam tubes were flooded with water at full density.

Results from the rest of the Co-V wire activation data are shown in Figures 27-30. For the low power experimental cores 176AXI, 177AXI and 179AX2 the results were used to obtain necessary safety approvals to operate cores 176A, 177A and 179A at full power. All of these cores were modeled with an explicit representation of the beam tubes with voids being replaced with water at 3% of normal density. As before, only wires irradiated in standard fuel elements were used to evaluate the RMS DEV values.

7.3 Differential and Integral Shim Rod Worths

It was pointed out in Section 6.2 that errors associated with the determination of the $n(t_2)/n(t_1)$ flux ratio limit the accuracy of the reactivity determination. In an effort to minimize these errors, the measured flux profile, corrected for counting losses and obvious noise spikes, was fit by the least squares process to a high degree polynomial in the range over which the flux ratios were to be determined. Three sets of flux ratios were evaluated at different times along this fitted curve. The three corresponding differential shim rod worths were then calculated by the methods described earlier and averaged to obtain the final result.

A	H ₂ O								
B	H ₂ O	H ₂ O	H ₂ O	H ₂ O	0.99	H ₂ O	H ₂ O	H ₂ O	H ₂ O
C	H ₂ O	H ₂ O	1.00	0.98 0.98	1.01 1.01	0.98 0.98	0.98	H ₂ O	H ₂ O
D	H ₂ O	H ₂ O	0.97 0.97	0.99 0.99	1.01 1.01	0.97 0.96	0.93 0.94	H ₂ O	H ₂ O
E	H ₂ O	0.98	1.02 1.02	1.02 1.02	1.02 1.02	1.01 1.02	0.98 0.98	0.99	H ₂ O
F	H ₂ O	H ₂ O	1.03 1.03	1.00 1.00	1.04 1.04	0.99 0.99	0.99 0.99	H ₂ O	H ₂ O
G	H ₂ O	H ₂ O	H ₂ O	H ₂ O	1.03	H ₂ O	H ₂ O	H ₂ O	H ₂ O
	1	2	3	4	5	6	7	8	9

DIF3D/VIM reaction rate ratios for neutron absorption (upper) and fission production (lower) in the ORR Core 179-AX5. Monte Carlo statistical errors are about 1.5% in the core and 2-3% in the water reflector.

Fig. 21

A	H ₂ O	H ₂ O	H ₂ O	H ₂ O	1.20	H ₂ O	H ₂ O	H ₂ O	H ₂ O
B	H ₂ O	H ₂ O	H ₂ O	H ₂ O	0.99	H ₂ O	H ₂ O	H ₂ O	H ₂ O
C	H ₂ O	0.94	0.95	0.95	0.96	0.96	0.95	0.95	H ₂ O
D	H ₂ O	0.96	0.96	0.97	1.00	0.97	0.99	0.96	H ₂ O
E	1.08	0.93	0.98	0.99	1.02	0.98	0.99	0.92	1.11
F	H ₂ O	0.88	0.99	1.00	1.02	0.99	0.98	0.88	H ₂ O
G	H ₂ O	0.95	1.04	1.07	1.06	1.06	1.05	0.96	H ₂ O
	1	2	3	4	5	6	7	8	9

DIF3D/VIM reaction rate ratios for neutron absorption (upper) and fission production (lower) in the ORR Core 179-AX6. Monte Carlo statistical errors are about 1% in the core, 2% in the beryllium reflector and 3-4% in the outer water reflector.

Fig. 22

ORR CORE LEU-1
 AVERAGE C/E RATIOS FOR IRRADIATED WIRES

	1	2	3	4	5	6	7	8	9
A	Water								
B	Water								
C	Water	Water	MFE	1.00	1.03	1.02	MFE	Water	Water
D	Water	Water	1.02	SR	1.08	SR	1.00	Water	Water
E	Water	Water	0.96	0.99	0.97	0.98	0.92	Water	Water
F	Water	Water	0.94	SR	1.12	SR	0.96	Water	Water
G	Water								

Fig. 24

RMS DEV = 0.051
 Fig. 24

ORR CORE 174-C
 AVERAGE C/E RATIOS FOR IRRADIATED WIRES
 NEW AND (ORIGINAL) COBALT-59 CROSS SECTIONS

	1	2	3	4	5	6	7	8	9
A	Be 1.25 (1.07)	1.13 (1.13)	1.17 (1.15)	1.16 (1.13)	1.17 (1.15)	1.03 (1.02)	1.07 (1.06)	1.08 (1.08)	Be 1.17 (1.01)
B	Be 1.20 (1.04)	Be 1.20 (1.04)	1.06 (1.08)	SR 1.10 (1.10)	0.98 (0.99)	0.99 (1.01)	0.99 (1.00)	Be	Be
C	Be 1.05 (0.90)	1.14 (1.14)	MFE	1.11 (1.12)	1.07 (1.08)	1.04 (1.04)	MFE	0.93 (0.91)	Be 0.92 (0.79)
D	Be	0.99 (0.99)	1.06 (1.06)	SR 1.09 (1.00)	1.02 (1.04)	1.00 (0.97)	0.94 (0.94)	0.87 (0.87)	Be
E	Be 1.07 (0.92)	1.04 (1.03)	HFED	1.00 (1.00)	IR	0.98 (0.99)	IR	0.91 (0.90)	Be 0.83 (0.71)
F	Be 1.13 (0.98)	Be 1.13 (0.98)	1.13 (1.01)	SR 0.92 (0.92)	0.97 (0.98)	SR 0.90 (0.90)	0.93 (0.93)	Be 0.96 (0.85)	Be
G	Be	Be	Be 1.06 (0.91)	Be 1.08 (0.92)	Be 1.07 (0.92)	Be 1.05 (0.92)	Be 0.98 (0.84)	Be	Be

New Co-59 XS's
 Original Co-59 XS's

Fig. 25

RMS DEV = 0.090 (0.083)
 Fig. 25

ORR CORE 179-A
Average C/E Ratios for Irradiated Wires

A	DF	Be	0.97	0.98	0.94	0.95	0.94	Be	DF
B	Eu	Ir	0.91	SR	0.90	SR	0.91	Ir	Eu
C	Be	1.01	MFE	0.98	0.97	0.98	MFE	0.90	Be
D	Eu	1.04	1.04	SR	0.99	SR	0.97	0.98	Eu
E	Be	1.02	Al	1.05	1.06	1.02	Ir	1.00	Be
F	Eu	Ir	1.03	SR	1.01	SR	1.08	Be	Eu
G	DF	Be	DF						
	1	2	3	4	5	6	7	8	9

RMS DEV = 0.050
FIG. 30

A typical set of data used to evaluate the differential shim rod worth is shown in Table 30. Note that delayed photoneutrons are needed to give a reasonable comparison between calculated and measured differential worths. Appendix E illustrates in considerable detail the evaluation of the differential shim rod worth for case 2 in Table 30 beginning with the measured time-dependent flux.

Semilog plots of calculated and measured flux profiles are compared in Fig. 31 for the B4 shim rod measured under low (1,200 gpm) and high (18,000 gpm) flow rate conditions in core 179AX7 (see Fig. 14). The calculated curves show the influence of transient terms at the beginning and the pure exponential shape in the asymptotic region near the end of the curves. Because of the finite time required to move the shim rod from the initial to the final position, the experimental curves fall above the calculated ones. Rod movement times for the low and high flow rate cases are 11.2 and 18.8 seconds, respectively. Therefore, the measured curve is closer to the calculated one for the low flow rate case. A careful examination of the experimental curves shows that because of increasing temperatures neither curve approaches a pure exponential. These temperature effects are smallest for the high flow rate case, as would be expected. For this particular set of data the % $\delta k/k$ /in. C/E ratios are 0.978 ± 0.052 (1200 gpm) and 0.966 ± 0.050 k (18,000 gpm). Even with very different temperature-related feedback effects, the methods described earlier give equally good differential shim rod worths.

The ANL-modified version of the PARET code⁴² was used to simulate positive reactivity insertions corresponding to the movement of the D4 shim rod in ORR core 179AX7. This code includes a treatment of the coupled thermal, hydrodynamic, and neutron kinetic properties of the core. For these simulations, the geometric model of the core, the fuel and cladding thermal conductivities and heat capacities, and the fuel and coolant temperature coefficient of reactivities were the same as those used for the transient safety studies for the ORR LEU demonstration cores. The purpose of these calculations was to investigate the relative importance of temperature-driven reactivity feedback effects and delayed photoneutrons on the shape of the flux transient following a slow positive reactivity insertion.

In the first simulation the D4 shim rod in core 179AX7 was withdrawn from 12.00 to 12.39 inches in 16.8 seconds corresponding to a calculated reactivity insertion of 0.1544 % $\delta k/k$. The coolant flow rate was 1,200 gpm with an inlet temperature of 25.5°C. For the second case the coolant flow rate was 18,000 gpm with an inlet temperature of 45°C while the D4 shim rod was displaced from 12.00 to 12.38 inches in 15.2 seconds. This corresponds to a calculated reactivity insertion of 0.1504 % $\delta k/k$. The delayed neutron kinetic parameters used in these PARET calculations were those given in Section 6.3.

Figs. 32 and 33 compare the results of these PARET simulations with the measured transients. It is clear from these figures that delayed photoneutron contributions are needed to better approximate the shape of the observed transients. However, the simulations tend to underestimate temperature-related feedback effects on the shape of the time-dependent fluxes.

Flux profile curves for small shim rod displacements were measured for each of the cores shown in Fig. 14. Using the methods described in Sections 6.2 and 6.3, differential shim rod worths were obtained for each of these cores from a careful analysis of the initial shape of these curves. The results⁴³ are summarized in Table 31. Generally speaking, measured and calculated differential shim rod worths agree reasonably well. However, the errors (1σ) are quite large. Most of these errors result from the statistical uncertainty with which the $n(t_2)/n(t_1)$ flux ratios were measured. In most cases these flux ratio errors were in the 3-4% range. At the time of these measurements it was thought that the asymptotic periods could be obtained directly from the final portions of the flux profiles. Therefore, the detector locations were chosen so as to give good counting statistics in the asymptotic region. Because of temperature effects, however, the initial

Table 30. Differential Worth of the D6 Shim Rod in ORR Core 179AX7

<u>Quantity</u>	<u>Case 1</u>	<u>Case 2</u>	<u>Case 3</u>
R_i - in.	12.00	12.00	12.00
R_f - in.	12.36	12.36	12.36
Flow rate, gpm	1200	1200	1200
Period Guess ^a , sec	42.0	42.0	42.0
t_1^b , sec	10.0	20.0	30.0
t_2^b , sec	30.0	40.0	50.0
$n(t,2)/n(t)$	1.62073	1.61574	1.59461
Stat. Err. in Ratio, %	2.92	2.56	2.27
T^c , sec	16.8	16.8	16.8
% $\delta k/k/in.$:			
Calc.	0.4287	0.4287	0.4287
Meas. no (γ,n)	0.351 ± 0.015	0.356 ± 0.015	0.353 ± 0.014
Meas. with (γ,n)	0.411 ± 0.017	0.420 ± 0.016	0.418 ± 0.017
C/E with (γ,n)	1.043 ± 0.042	1.021 ± 0.040	1.027 ± 0.040

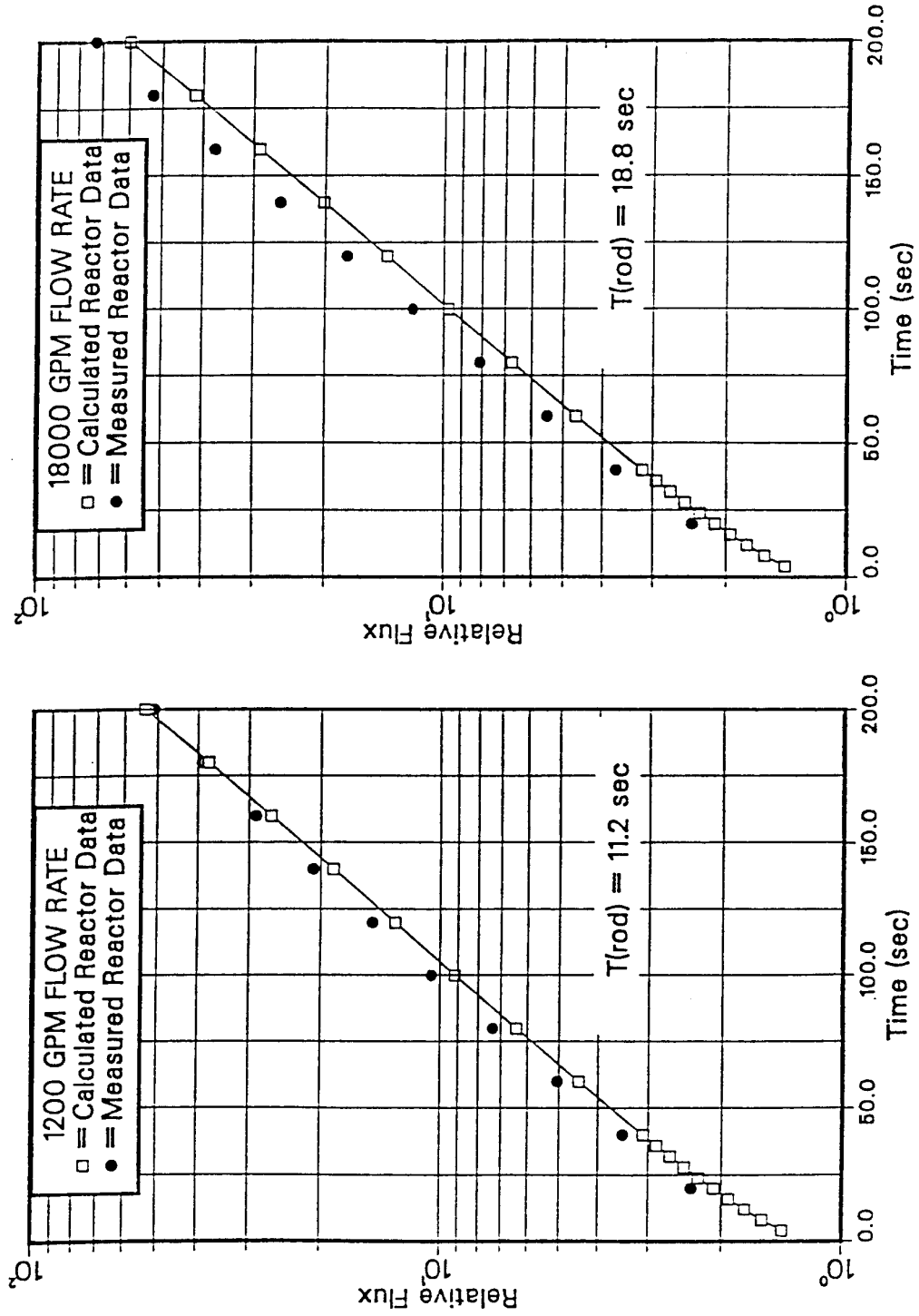
^aThe initial asymptotic period guess is taken as the e-unfolding time recorded with a stop watch at the time of the measurement.

^bThese times are measured with respect to the end of the rod motion.

^cT is the time for the rod displacement from R_i to R_f .

RELATIVE FLUX FOLLOWING B4 SHIM ROD MOVEMENT

ORR CORE 179-AX7



Note: $T(\text{rod}) \equiv$ time for rod to move from R_i to R_f .
 FIG. 31

DIFFERENTIAL ROD CALIBRATION POWER TRACE

ORR Core 179-AX7 - Rod D4

Reactor Coolant Flow - 1200 GPM

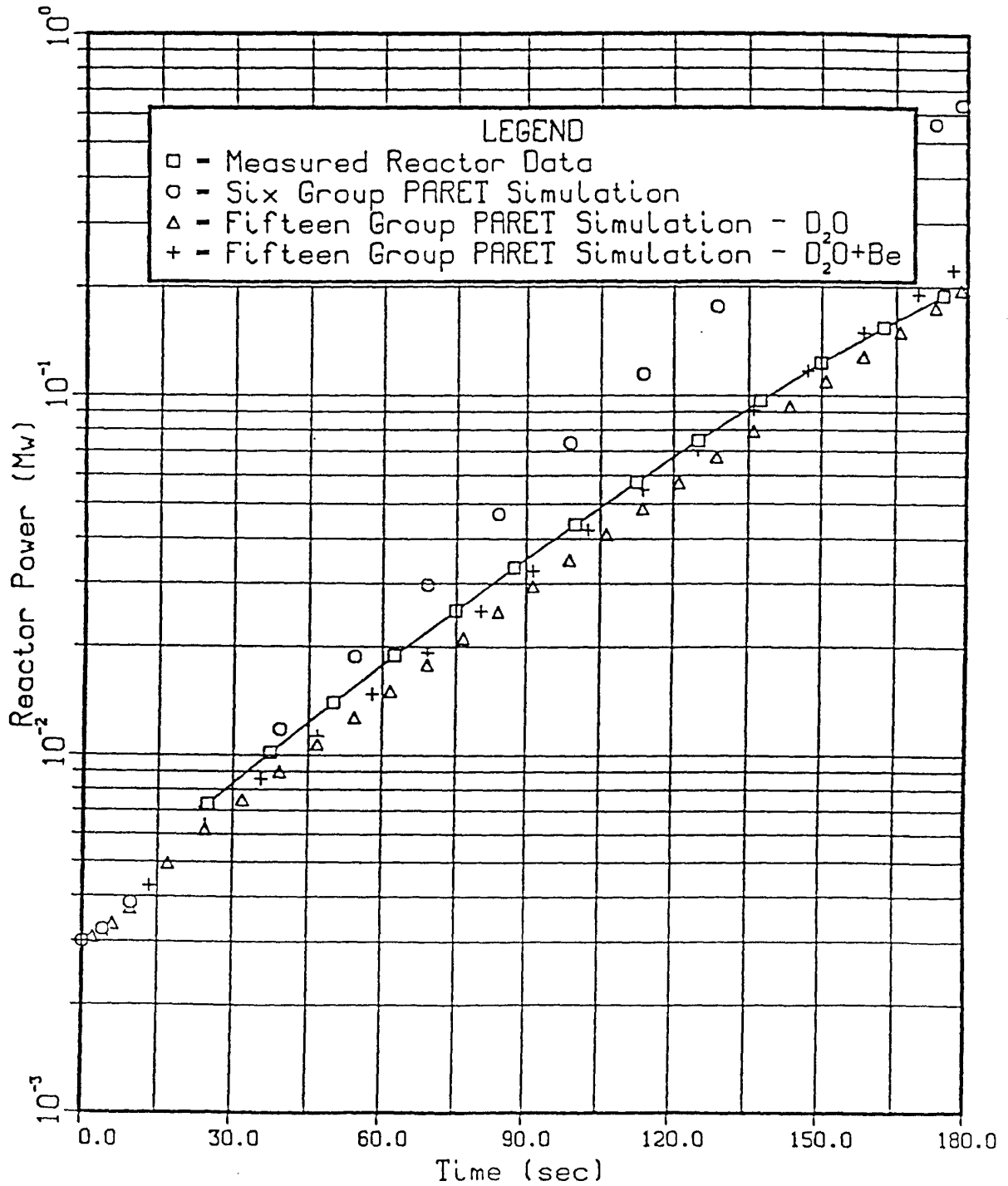


FIG. 32

DIFFERENTIAL ROD CALIBRATION POWER TRACE

ORR Core 179-AX7 - Rod D4

Reactor Coolant Flow = 18000 GPM

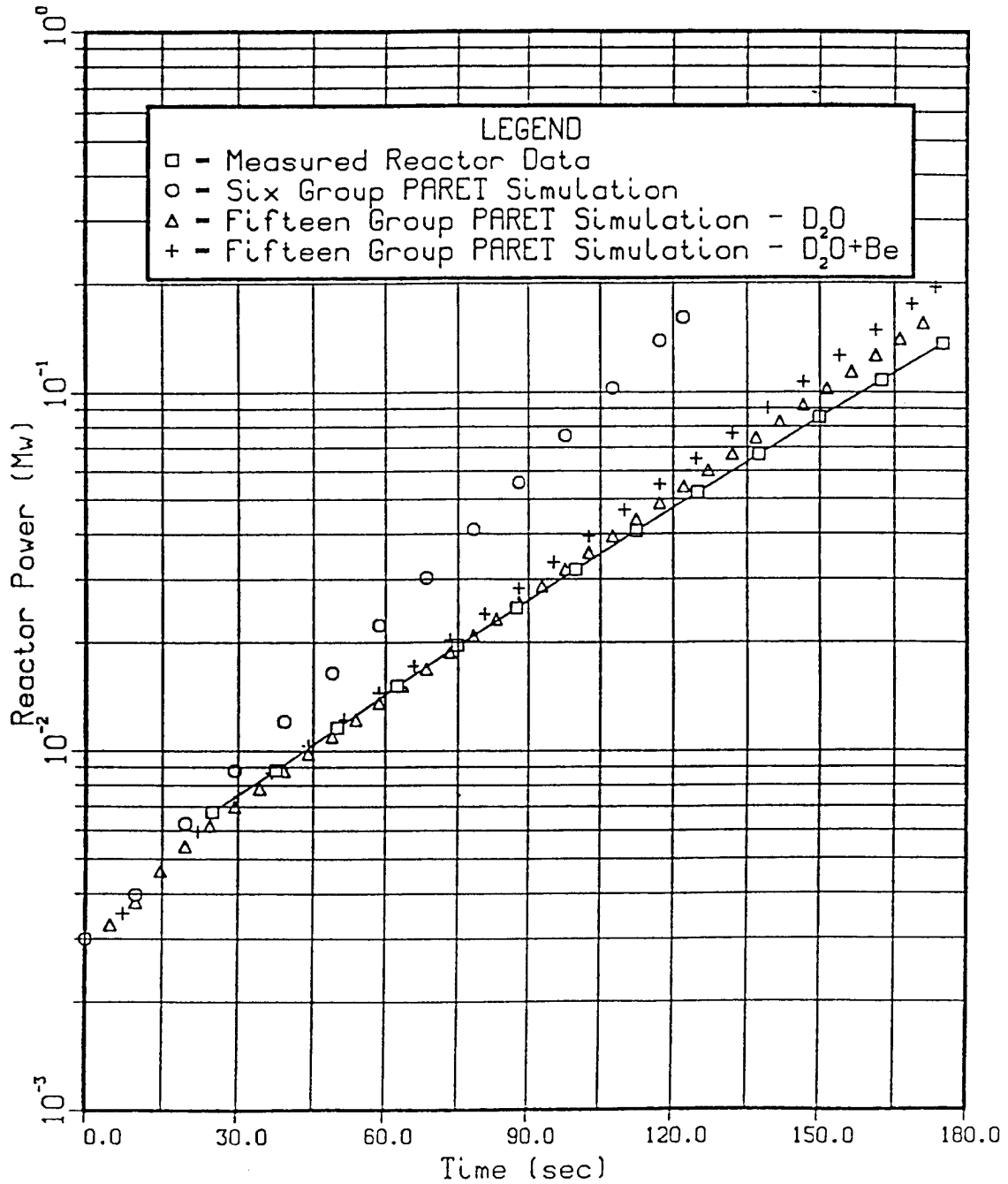


FIG.33